13th ewtec 2019 Proceedings of the 13th European Wave and Tidal Energy Conference 1-6 Sept 2019, Naples, Italy

Modelling Wave Interaction with thin porous Structures using OpenFOAM

Anna Feichtner, Ed B. L. Mackay, Gavin Tabor, Philipp R. Thies, Lars Johanning

Abstract— **In coastal and ocean engineering porous structures are often used to dissipate the energy of incoming waves onto fixed or floating bodies. This work is an initial step to investigate the application of a porous shroud around the platform of floating offshore wind turbines or similar marine renewable energy systems.**

Most Computational Fluid Dynamics (CFD) models for porous structures have focused on large-volume porous structures such as concrete or rubble-mound breakwaters. In contrast to that, this paper looks at thin porous structures, such as perforated steel plates. It presents the development of a robust set-up for a numerical wave tank (NWT) and an assessment of the use of CFD for modelling the wave interaction with fixed thin porous sheets.

For the CFD simulations, the open-source code OpenFOAM was used together with the OlaFlow toolbox, which provides wave modelling methods as well as a macroscopic porosity implementation.

The main objective is to analyse the wave interaction with fixed vertical porous sheets in regard to the pressure loss across the sheet. Basic studies are carried out to achieve a robust set-up of a NWT including thin porous media, which can be used for further, more detailed studies. The CFD simulations are compared against measurements from tank test results.

Keywords—**CFD, OlaFlow, OpenFOAM, thin porous structures, wave structure interaction**

I. Introduction

VARIOUS offshore marine structures consist of one or more floating bodies. One engineering challenge is to develop a structure, which will be stable under operational and extreme wave conditions. A promising approach to improve the performance of floating structures is the application of a porous outer layer in order to dissipate energy and function as a passive damping system. This mechanism is similar to Jarlan-type breakwaters and has the potential to improve the motion response characteristics and to reduce the wave loads as well as the mooring forces. One promising use in the field of marine renewable energy systems is its application to floating offshore wind turbine platforms.

This paper presents the first steps in the development of a robust numerical wave tank (NWT) for modelling wave loads on thin porous structures. The current work focuses on fixed porous plates and will be further developed to a floating set-up later on.

The C++ based open-source code OpenFOAM (hereafter OF) was used in combination with the OlaFlow toolbox [1]. OlaFlow provides wave generation boundary conditions, an active wave absorption technique as well as a macroscopic porosity application for interaction in the coastal and offshore fields. For the implementation of porous zones, it uses a transient volume-averaged Reynolds-averaged Navier-Stokes (VARANS) approach in combination with additional sink/closure terms in the governing momentum equation. The flow through porous elements is modelled using a parametric pressure-flow relation. The alternative to a macroscopic approach would be a microscopic porosity implementation, where the flow through each perforation in the porous material is modelled explicitly. This requires a highly detailed representation of the porous geometry and entails a significantly higher computational cost, making it unfeasible for most ocean engineering applications.

OlaFlow is mainly used for large-volume porous zones, such as concrete-block or rubble mound breakwaters, e.g. in [2]. In contrast, this paper presents the validation of the code for wave interaction with thin porous structures.

Wave tank tests were conducted to help the numerical modelling, both the current CFD models as well as a BEM model as described in [3]. The tests addressed two-dimensional conditions involving thin perforated plan

ID-number: 1415; Conference track: Wave hydrodynamic modelling; This work was supported as part of the EPSRC (UK) grant for the project "Resilient Integrated-Coupled FOW platform design methodology (ResIn)" [grant number EP/R007519/1].

A. Feichtner (e-mail: af506@exeter.ac.uk), E.B.L. Mackay (e-mail: e.mackay@exeter.ac.uk), P.R. Thies (e-mail: p.r.thies@exeter.ac.uk) and L. Johanning (e-mail: l.johanning@exeter.ac.uk) are with the Renewable Energy Research Group, College of Engineering, Mathematics & Physical Sciences, University of Exeter, Penryn, Campus, Penryn, TR10 9FE, UK.

G. Tabor (e-mail: g.r.tabor@exeter.ac.uk) is with the Engineering Group, College of Engineering, Mathematics & Physical Sciences, University of Exeter, Streatham Campus, Exeter, EX4 4PY, UK.

sheets. The CFD results are compared against the tank test data.

Potential-flow theory can be used to model the wave interaction with porous structures. For instance, previous work in the context of fixed and floating breakwaters has been done by [4] and [5] and motion damping of fixed and floating structures by [6], [7] and [8]. A comparison of a potential flow model for flat porous sheets with the tank test data considered in this work is presented in [9].

This paper is structured as follows. The experimental setup is presented in Section II, the CFD method is described in Section III and the CFD model setup in Section IV. Comparisons between the CFD model and tank tests are presented in the Sections V. Finally, conclusion are presented in Section VI.

II. EXPERIMENTAL METHOD

Tank tests were conducted at Dalian University of Technology (DUT), China, to investigate the effects of various geometrical parameters and wave conditions on the wave-structure interaction. The resulting data is used for the validation of numerical methods, particularly an in-house BEM code for porous structures [3,10] as well as for the CFD models with macroscopic porous media.

A. Wave Flume and Test Setup

The DUT wave flume has a length of 60m, is 4m wide and has a variable water depth up to a maximum water depth of 2m. The tank has a single piston-type paddle and is capable of generating regular and irregular waves. Opposite to the paddle, a beach is located to absorb the incident waves. For the 2D test runs, the flume was divided to give a section of 1m width.

To simplify the setup, tests were conducted with porous sheets that filled the entire water column. The porous sheets were mounted on a rigid frame, which was connected to load cells at the top and bottom. A temporary raised floor was installed in a section of the tank, so that the lower load cell could be submerged beneath the tank floor. A sketch of the ramp geometry is shown in Fig. 1. To avoid load transfer between the screen and the tank, a small separation distance of 5mm was left between the porous screen, sidewalls and the tank floor. The water depth at the location of the porous sheet was 1m. The porous sheets were 1.5m high, to ensure that no over-topping occurred.

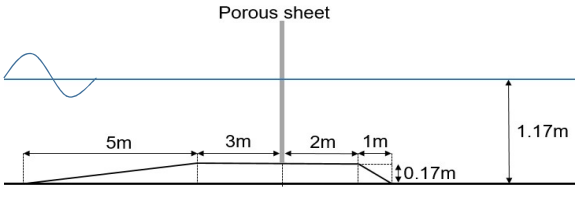

Fig. 1: Sketch of bottom ramp of wave tank experiments

TABLE I
SPECIFICATIONS OF POROUS SHEETS USED IN TANK TESTS

Porosity n [-]	Spacing s [mm]	Thickness Δx [mm]
0.1	25	3
0.2	25	3
0.3	25	3
0.4	25	3
0.2	33.3	3
0.2	50	3
0.2	100	3
0.2	25	6
0.2	25	10
0.2	50	6
0.2	50	10

B. Test parameters

The tank tests aimed to analyse the wave structure interaction in a two-dimensional setting involving vertical perforated plates that filled the entire water column in a narrow flume. The sheets contained a regular grid of holes of radius r, with hole centres separated by distance s. The sheet's porosity n is defined as the ratio of void area to total area as

$$n = \pi r^2 / s^2 \tag{1}$$

The tests covered a range of values of porosity n, hole spacing s and plate thickness Δx (see Table I) under a series of regular and irregular wave conditions. The regular waves had nondimensional wavenumbers in the range $0.6 < kh < 3.4$ (where k is the wavenumber and $h =$ 1m is the water depth at the porous sheet) and steepnesses in the range $0.05 \leq kA \leq 0.20$ (where A is the wave amplitude).

For the CFD simulations, a limited number of regular wave conditions were selected. Table II shows the selected conditions, where T represents the wave period, λ the wavelength and H the wave height. Each condition was analysed for a flat tank bottom with a water depth of h=1.00m.

TABLE II
SELECTED WAVE CONDITIONS FOR CFD SIMULATIONS

Wave Cond.	T[s]	λ[m]	H[m]
F2	1.3	2.60	0.0413
F3	1.5	3.35	0.0533
F6	2.1	5.58	0.0887
F9	2.7	7.67	0.1221
F10	2.9	8.35	0.1330

C. Anomalies in Results

The results of the tank tests have been compared against potential flow models [9]. An unexpected behaviour was observed at some wave frequencies (including F9 and F10 as in Table II), where there was a large difference between the experimental results and numerical predictions. It was suspected that this was due to the wave interaction with the raised section of the tank floor. To investigate this, CFD simulations have been conducted for selected wave conditions with both a flat bottom and a raised floor, see Section IV.

III. CFD METHOD

For the CFD simulations, the C++ based open-source code OpenFOAM (OF Foundation Version 5) was used in combination with the OlaFlow toolbox.

D. Governing Equations

OF utilises the finite volume method for solving the Navier-Stokes (NS) equations, which is an Eulerian approach with evaluation of the fluxes through fixed control volumes. A transient Reynolds-Averaged-Navier-Stokes (RANS) approach was used for this work. The conventional RANS governing equations for incompressible fluids, which is widely used for coastal engineering problems [10], are the mass conservation equation

$$\nabla \cdot \boldsymbol{U} = 0 \tag{2}$$

and the momentum equation

$$\begin{aligned}\frac{\partial \rho \boldsymbol{U}}{\partial t} + \nabla \cdot (\rho \boldsymbol{U}\boldsymbol{U}) - \nabla \cdot \left(\mu_{eff} \nabla \boldsymbol{U}\right) \\ = -\nabla p^* - \boldsymbol{g} \cdot \boldsymbol{X} \nabla \rho + \nabla \boldsymbol{U} \\ \cdot \nabla \mu_{eff} + \sigma \kappa \nabla \alpha\end{aligned} \tag{3}$$

where $\boldsymbol{U}$ represents the velocity vector, $\boldsymbol{X}$ the Cartesian position vector and $\boldsymbol{g}$ the gravitational acceleration vector. ρ denotes the weighted averaged density, calculated from the densities of water ρ_w and air ρ_a as $\rho = \alpha\rho_w + (1-\alpha)\rho_a$, where α is the fraction of water per unit volume in each cell, where $\alpha = 1$ corresponds to a cell full of water and $\alpha = 0$ to a cell full of air. Consequentially, α values between 0 and 1 represent a part of the phase interface. μ_{eff} is the effective dynamic viscosity, which is calculated by the molecular/dynamic viscosity μ and the turbulent viscosity ν_{turb} given by RANS turbulence models as $\mu_{eff} = \mu + \rho \cdot \nu_{turb}$. The dynamic pressure p^* is calculated as the difference of the total pressure p and the hydrostatic pressure: $p^* = p - \rho \boldsymbol{g}\boldsymbol{X}$. The last term of (3) corresponds to surface tension effects with σ as the surface tension coefficient and κ as the curvature of the interface.

E. Free surface Modelling Technique

OF uses the Volume of Fluid (VOF) method [11], to capture the free surface of the interface between the two phases air and water. As part of the VOF method, a so-called indicator phase function using the α –field (described above) is applied in the governing equations and solver respectively, which is defined as

$$\frac{\partial \alpha}{\partial t} + \nabla \cdot \boldsymbol{U}\alpha + \nabla \cdot \boldsymbol{U_c}\alpha(1-\alpha) = 0 \tag{4}$$

The last term in (4) helps to reduce numerical diffusion at the interface and sharpens it via the artificial so-called compression velocity $\boldsymbol{U_c} = \boldsymbol{U_l} - \boldsymbol{U_g}$ [12]. $\boldsymbol{U_c}$ is the difference between the velocity of the liquid phase $\boldsymbol{U_l}$ and the velocity of the gas phase $\boldsymbol{U_g}$. This compression term only acts at the interface ($0 < \alpha < 1$) to keep the interface "compressed", as $\boldsymbol{U_c}$ is zero when $\alpha < 0$ or $\alpha > 1$. In OF the boundedness of the solution of scalars, such as phase or mass fractions, is provided by the MULES (Multidimensional Universal Limiter for Explicit Solution) scheme [13].

An improved interface capturing approach is also available in OF and OlaFlow, called the IsoAdvector [14] algorithm, and will be considered for future work.

F. Wave Generation and Absorption

The OlaFlow toolbox provides various wave generation techniques as well as an active wave absorption technique. For the wave generation at the inlet, the boundary face is divided into a dry and a wet area, divided by the phase interface. The velocity profile $\boldsymbol{U}$ and the volume fraction α are imposed based on the selected wave theory. A Stokes 2nd order formulation has been used in this work.

The active wave absorption technique works by constantly adjusting the boundary conditions with a correction velocity and a corrected phase fraction at both the inlet and outlet. This aims to cancel out wave reflection. At the inlet, the target elevation conforms to the theoretical elevation based on the applied wave theory; at the outlet, the adjustment uses the still water level.

At the moment, this technique is implemented based on shallow water theory, which implies a constant vertical velocity profile through the water column [15]. Consequently, the applicability of this absorption method decreases with increasing water depth.

G. Porosity Implementation

In general, porous media can be implemented in CFD in a microscopic or macroscopic manner. A microscopic implementation is realised by a detailed geometry resolution, which means an exact representation of every void or solid. This entails a high computational cost, as the computational mesh needs to be resolved in fine detail. For most engineering applications, this is not feasible nor necessary and a macroscopic approach can be used instead.

The macroscopic porosity implementation is represented by an averaged pressure loss through the porous media, where the detailed geometry does not need to be resolved. The pressure loss is accounted for by

adding sink-terms to the momentum equation, which are only used in the geometric region of the porous media.

The pressure loss ΔP across a thin porous barrier can be expressed as [16]:

$$\frac{\Delta P}{\rho} = \frac{\nu U_n}{l} + \frac{C_f}{2} U_n |U_n| + c \frac{\partial U_n}{\partial t} \tag{5}$$

where l is a length scale (related to sheet thickness, hole size, etc.), c is an inertial coefficient with the dimension of length, C_f is a dimensionless friction coefficient and U_n is the average velocity normal to the porous sheet.

Dependent on the flow regime through porous media, any of the three terms becomes either dominant or negligible. The linear viscous friction term governs for low Reynolds-numbers and the nonlinear turbulent dissipation term is dominant for high Reynolds-numbers [16]. The third transient term accounts for added mass effects and transient interaction between the fluid and the porous medium.

OlaFlow [1] uses an alternative formulation of (5) where the pressure loss is expressed in terms of a hydraulic gradient I, defined as the change in pressure per unit length Δx:

$$I = \frac{\Delta P}{\Delta x} = A U_D + B U_D |U_D| + C \rho \frac{\partial U_D}{\partial t} \tag{6}$$

where $\boldsymbol{U_D}$ represents the Darcy velocity, which is defined as the equivalent flow velocity per unit cross-sectional area of the porous medium. In this case, the Darcy velocity U_D is equal to the average velocity normal to the porous sheet U_n as in (5). The coefficients A, B and C are defined in OlaFlow as:

$$A = \alpha \frac{(1-n)^3}{n^2} \frac{\mu}{D_{50}^2} \tag{7}$$

$$B = \beta \left(1 + \frac{7.5}{KC}\right) \frac{1-n}{n^3} \frac{\rho}{D_{50}} \tag{8}$$

$$C = \frac{c}{\Delta x} \tag{9}$$

for the linear and quadratic terms, where Δx is the sheet thickness, D_{50} is the mean nominal diameter of the material, which is usually grain or particle shaped and KC is the Keulegan-Carpenter-number. In the present work, the grain diameter has no physical meaning and its value is set to 1.0.

It is worth noting that if the switch "useTransient" is set to "true" in OlaFlow's porosityDict dictionary, the term $\frac{7.5}{KC}$ in (8) is included with a default value for KC of 1.0, otherwise this term is set to zero. The latter corresponds to using Engelund's [17] formulation, the former corresponds to using Van Gent's [18] modification. However, these definitions were derived for flow through thick porous structures such as rubble or concrete mounds. For thin porous barriers, different flow mechanisms are dominant and an alternative formulation is used, as discussed below.

The coefficients α, β and c are the default input parameters in OlaFlow, which typically need to be calibrated in the CFD model [10]. However, for thin perforated sheets, the physical meaning of (7) and (8) become irrelevant and (5) can be used instead of (6). As D_{50} and KC have no physical meaning here, both were set to 1.0 (using the Van Gent formula) for the current studies, resulting in the following expressions for α and β:

$$\alpha = \frac{n^2}{l \Delta x (1-n)^3} \tag{10}$$

$$\beta = \frac{n^3 C_f}{17 \Delta x (1-n)} \tag{11}$$

In this work, the model of Molin [8] is used for the drag coefficient C_f, defined as

$$C_f = \frac{1-n}{\delta n^2} \tag{12}$$

where δ is a discharge coefficient. In the present work a constant value of $\delta = 0.5$ is assumed.

Within the porous medium, the standard RANS momentum equation (3) must be modified to account for the limited amount of fluid and the pressure gradient (6). The resulting volume-averaged RANS equation (VARANS) can be written as [10]:

$$\begin{aligned} (1+c)\frac{\partial}{\partial t}\frac{\rho \boldsymbol{U_D}}{n} + \nabla\left(\frac{\rho \boldsymbol{U_D} \boldsymbol{U_D}}{n^2}\right) &= -\nabla p^* \\ -\boldsymbol{g} \cdot \boldsymbol{X} \nabla \rho + \nabla \cdot \left(\mu_{eff} \nabla \frac{\boldsymbol{U_D}}{n}\right) + \sigma \kappa \nabla \alpha - A \frac{\boldsymbol{U_D}}{n} & \\ - B \frac{\boldsymbol{U_D}}{n} \left|\frac{\boldsymbol{U_D}}{n}\right| & \end{aligned} \tag{13}$$

where $\frac{\boldsymbol{U_D}}{n}$ represents the intrinsic velocity, which is the actual fluid velocity inside the voids of the porous media.

The VARANS equations are combined with a modified MULES–term in the VOF-equation (4) as well as adapted and volume-averaged turbulence models - all constraining the amount of fluid that can enter each mesh cell. The altered $k-\varepsilon-$ and $k-\omega-SST$ models can be found in [10].

H. Flow State and Turbulence Modelling

A laminar flow model has been used for the entire computational domain. The justification for this is as follows. Firstly, the turbulent dissipation in the vicinity of the porous plate is already accounted by the turbulent sink term in the macroscopic porosity model. Therefore, the use

of a turbulence model would result in an additional turbulent loss [19].

Secondly, outside the porous region, the tank floor is smooth enough to assume a slip condition. Additionally, the gradient of the raised floor is sufficiently low so that flow separation is unlikely to occur at the transition.

I. The OlaFlow Solver

The OlaFlow solver is based on OF's standard interFoam solver, which is developed to solve the unsteady RANS equations for two incompressible phases. Both use the merged PISO-SIMPLE solver algorithm, the so-called PIMPLE algorithm for the pressure-velocity coupling.

The OlaFlow solver uses the VARANS-equation inside the porous media. Outside the porous area, the VARANS-equations are equal to the standard RANS- equations and the OlaFlow solver is equivalent to the interFoam solver.

IV. CFD SIMULATIONS

J. Model Setup

1) Computational Domain and Mesh

Simulations were conducted both with and without the porous sheet in the water. The simulations without the porous sheet were used to examine the mesh convergence around the free surface.

The domain length of the NWT was defined as 26m and for the cases with the porous sheet, the sheet was positioned in the middle of the domain, to maximise the time before reflected waves arrive from either the inlet or outlet. As OF requires a three-dimensional mesh, the width in the cross-direction was set to 1cm with a single cell.

Fig. 2 shows the NWT schematically with the waves travelling from the inlet on the left side to the outlet on the right side.

2) Boundary Conditions

For the regular wave conditions, 2nd-order Stokes (StokesII) waves were applied at the inlet. The free surface elevation η is defined as

$$\eta = \frac{H}{2}\cos(\theta) + k\frac{H^2}{4}\frac{3-\sigma^2}{4\sigma^3}\cos(2\theta) \tag{14}$$

where $\sigma = \tanh(kh)$ and $\theta = kx - \omega t + \psi$ with h as the water depth, H as the wave height, k as the wave number, θ as the wave phase, ω as the angular frequency, ψ as the phase, x the horizontal coordinate and t as the time.

The horizontal and vertical velocity components U and W are

$$U = \frac{H}{2}\omega\frac{\cosh(kz)}{\sinh(kh)}\cos(\theta) + \frac{3}{4}\frac{H^2\omega k\cosh(2kz)}{4\sinh^4(kh)}\cos(2\theta) \tag{15}$$

and

$$W = \frac{H}{2}\omega\frac{\sinh(kz)}{\sinh(kh)}\sin(\theta) + \frac{3}{4}\frac{H^2\omega k\sinh(2kz)}{4\sinh^4(kh)}\sin(2\theta) \tag{16}$$

The top boundary was set to an atmospheric condition; the bottom boundary was set to a wall with a slip-condition, as the roughness can be assumed to be negligible.

As the models are two-dimensional, the front- and back boundaries are set to an empty condition, which is the standard method for 2D cases in OF.

3) Porosity Characteristics

For the implementation of the porous sheet, a 1cm thick area with a porosity of $n = 0.1$ reaching over the complete domain height was applied in the middle of the domain. The porosity coefficients of the linear and transient term were set to $\alpha = c = 0$. The coefficient for the quadratic term β was calculated with (11) for $n = 0.1$ and Δx=1.0cm using (12) to $\beta = 1.1765$.

4) Solver Settings

For the temporal discretisation in CFD solvers, the Courant-Friedrich-Levy number Co influences the convergence. The Co number is defined as the number of cells that a scalar moves forward within one time step, e.g.

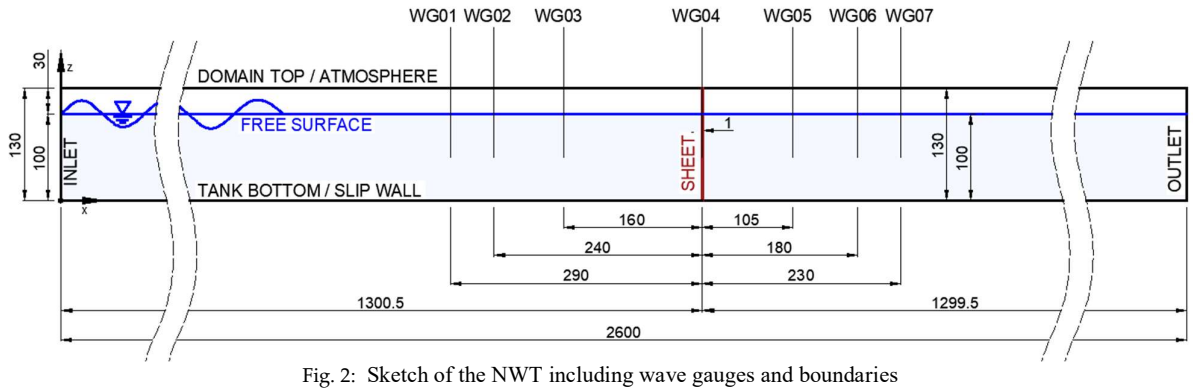

Fig. 2: Sketch of the NWT including wave gauges and boundaries

$Co = 0.5$ means that the fluid moves through (maximum) half a cell within one time step. For the modelling of ocean waves, relatively small Co -numbers are required for a sufficient resolution and capturing of the transient flow field. Therefore, the solver was set to an automatic time-step adjustment with a target maximum Co -number. For the empty NWT Co is set as 0.5, whereas for the cases with the porous sheet Co is reduced to 0.3-0.4 for a more stable solver run, as problems occurred with the coarser time step. The initial time step was set to 0.001s.

The main advantage of the PIMPLE algorithm of the OlaFlow/interFoam solver is the possible use of high Co -numbers to increase the speed of the simulations. However, with the requirement of small Co -numbers for wave modelling, the benefit becomes less relevant. Consequentially, OlaFlow is run with only one outer (SIMPLE) pressure-momentum correction-loop. The number of inner (PISO) pressure correction loops was set to a value of 3.

The residuals, which are the typical measure for an iterative solution's convergence as the imbalance of the solution of the set of equations, have been monitored. For all the simulations, the root-mean-square (RMS) of the local residuals dropped from a magnitude of 10^{-5}/10^{-3} to 10^{-8}/10^{-7} within each time step. Hence, the solution can be considered as converged at each time step.

The simulation time was between 35s and 55s to provide at least 10 wave periods to pass through the porous sheet, excluding an initial wave ramp-up period.

K. *Mesh Characteristics*

All the meshes consist of a regular hexahedral (HEX) base mesh in the general domain region created with OF's blockMesh functionality. The cell size of the base mesh in the general domain was set to 2.0cmx2.0cm. One comparative simulation with a cell size of 1.0cmx1.0cm showed that a generally finer mesh has no influence on the free surface elevation around the plate area. In the relevant refinement regions the refineMesh command was used, which splits the cell sides into halves for each execution.

Two sets of mesh convergence studies were conducted, each for the wave conditions F2 and F9 (see Table II). The first study analysed the free surface elevation at WG04 by adjusting the refinement at the vicinity of the free surface region. The second study analysed the pressure drop across the porous sheet in regard to the refinement around it.

1) *Convergence Study at the Free Surface Region*

For the initial mesh convergence for the free surface region, an empty NWT was setup for four meshes with the characteristics as in Table III. l_x and l_z represent the cell side lengths of the mesh cells in the refinement region along the free surface, which has a height of 24cm to cover a wide range of wave heights. The spatial discretisation at the vicinity of the phase interface was conducted regarding CPH (cells per wave height) and CPL (cells per wavelength).

TABLE III
MESH CONVERGENCE STUDY – FREE SURFACE REGION: MESH SPECS.

Mesh	No. Cells	Cell Dim. l_x [cm]	Cell Dim. l_z [cm]	Wave F2 CPL	Wave F2 CPH	Wave F9 CPL	Wave F9 CPH
1	97500	2.0	1.0	130	4.13	383.5	12.21
2	123500	1.0	1.0	260	4.13	767	12.21
3	175500	1.0	0.5	260	8.26	767	24.42
4	487500	0.5	0.25	520	16.52	1534	48.84

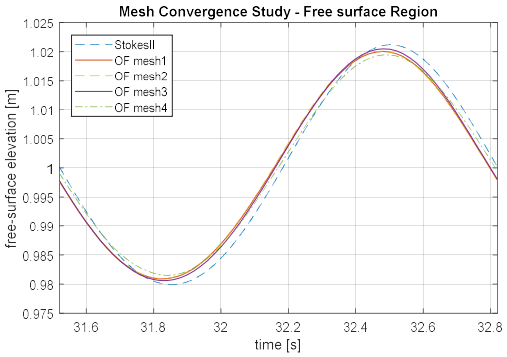

Fig. 3: Section of the time series of the free surface elevation for wave F2 at WG04 as part of the mesh convergence study at the free surface region including the target StokesII- elevation

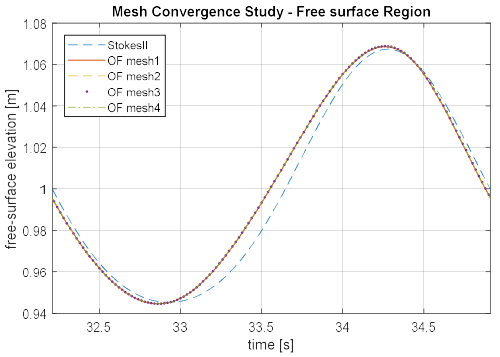

Fig. 4: Section of the time series of the free surface elevation for wave F9 at WG04 as part of the mesh convergence study at the free surface region including the target StokesII- elevation

Examples of the free surface elevation from the four meshes are shown in Fig. 3 and Fig. 4. As well as visual comparison of the free surface elevation, a second parameter was used to characterise the mesh convergence: the average amplitude A_{Eta} of the last 10 wave periods of the time series. This section of the record also includes some reflected waves, but was used to average out some of the temporal fluctuations in the wave amplitude. Table IV lists A_{Eta} for each mesh as well as the target amplitude for the wave conditions F2 and F9.

The mesh selected for use is highlighted in Table III, Table IV and Table V. This mesh was considered to be sufficiently accurate as the wave amplitude A_{Eta} changes less than 5% and the maximum amplitude difference of 0.09cm is significantly smaller than the cell height of l_z=0.5cm.

TABLE IV
MESH CONVERGENCE STUDY – FREE SURFACE REGION:
AVG. AMPL. A_{ETA} [CM]

Mesh	F2	F9
1	1.93	6.18
2	1.94	6.18
3	1.98	6.17
4	1.89	6.17
Target Ampl.	2.07	6.11

Consequently, all further models were set-up with a cell size of 2.0cmx2.0cm for the base mesh and 1.0cmx0.5cm for the free surface region. This gives a minimum CPH of 8 and CPL of 260 for the wave conditions considered. The values of 8 CPH and 260 CPL conform with the range of spatial discretisation used in other studies, such as [20, 21, 22, 23].

2) Convergence Study around Porous Sheet

As the analysis of the pressure drop through the porous sheet is the main objective, a second mesh convergence study of the area around the sheet was conducted analysing the pressure drop itself, again for the waves F2 and F9. Table V shows the mesh characteristics with $l_x = l_z$ as the cell size around the porous sheet. The refinement around and inside the plate was generated by gradually splitting the cells, in order to provide a smoother transition regarding the cell size growth rate. It is important to note that OF stores the parameter values at the cell centres. To calculate the pressure drop across the plate surface requires interpolation of the pressures onto the cell faces. Hence, the porous area has to consist of at least two cells in the x-direction. In the present study, the porous zone was kept at a constant width of 1cm and the number of cells was progressively refined.

TABLE V
MESH CONVERGENCE STUDY – PLATE REGION:
MESH SPECS. AND AVG. AMPL. A_{FORCE} [N]

			A_{Force} [N]	
Mesh	No. Cells	l_x, l_z [cm]	F2	F9
1	177777	1.0	0.585	4.669
2	185415	0.5	0.629	5.198
3	219547	0.25	0.617	5.440
4	293335	0.125	0.640	5.737
5	567895	0.0625	0.665	5.877

Fig. 5 shows the mesh section around the plate with a close up of the refinement regions around the free surface for the final mesh 5 (highlighted in Table V).

The total pressure field was calculated as the sum of the static pressure and the dynamic pressure. The total pressure was used to calculate the horizontal force as the difference of the integrated pressure values at the back and the front surface of the porous sheet. Fig. 6 and Fig. 7 show sections of the time series of the force on the plate for the wave conditions F2 and F9 and indicate a close agreement between results from mesh 4 and mesh 5.

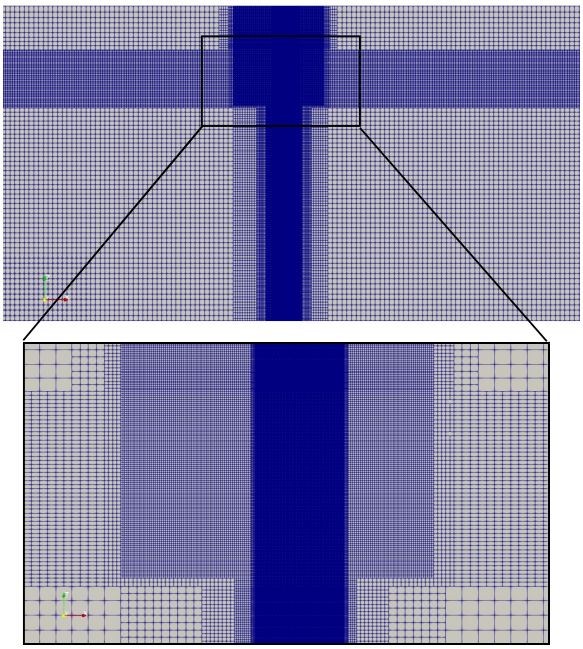

Fig. 5: Section of the mesh around the plate with close up, showing the refinement along the free surface area and around the vertical plate

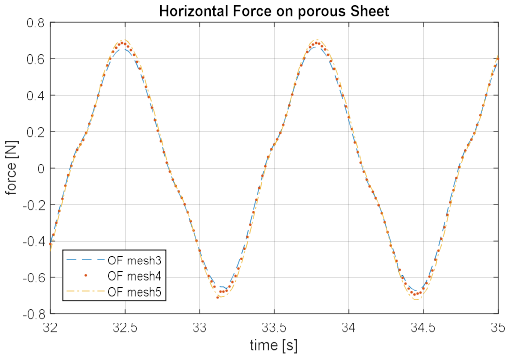

Fig. 6: Section of the time series of the horizontal force on the plate for wave F2 as part of the mesh convergence study around the plate region (showing only meshes 3-5)

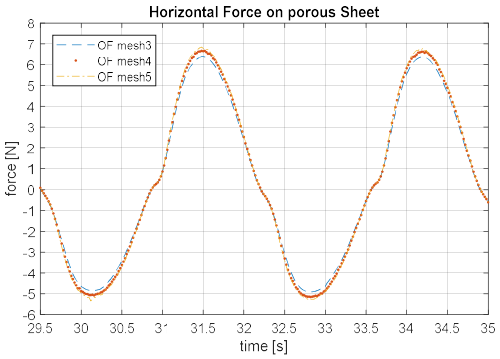

Fig. 7: Section of the time series of the horizontal force on the plate for wave F9 as part of the mesh convergence study around the plate region (showing only meshes 3-5)

Similar to the mesh study for the free surface region, the average force amplitude A_{Force} of the last 10 wave periods was analysed (which also includes the influence of some reflected waves).

Table V shows the average force amplitude A_{Force} for each mesh for the wave conditions F2 and F9. The results obtained by mesh 5 were considered sufficiently accurate as the change of the average force amplitude A_{Force} is less than 4%. Hence, a cell size of 0.0625cmx0.0625cm around the porous sheet was selected for all further models.

3) Reflection Coefficients in the NWT

The reflection coefficient was calculated for an empty domain for the selected free surface refinement of mesh 3 (Table III) using the wave condition F9 and the wave gauges WG 05, 06 and 07 as those are the closest ones to the outlet boundary (see Fig. 2). The Mansard and Funke 3-point-method [24] was used to analyse the wave elevation time series after removing the wave ramp-up and the initial transient response. For the wave F9 the reflection coefficient is 6.1%, which is considered to be sufficiently small for these studies. However, an enhanced absorption technique will be considered for future models.

V. Results

The CFD results for the model with a flat tank bottom were compared to the tank test data for selected wave conditions (see Table II). Fig. 8 shows the time series of the force onto the porous sheet for each wave condition considered and Table VI lists the average force amplitudes

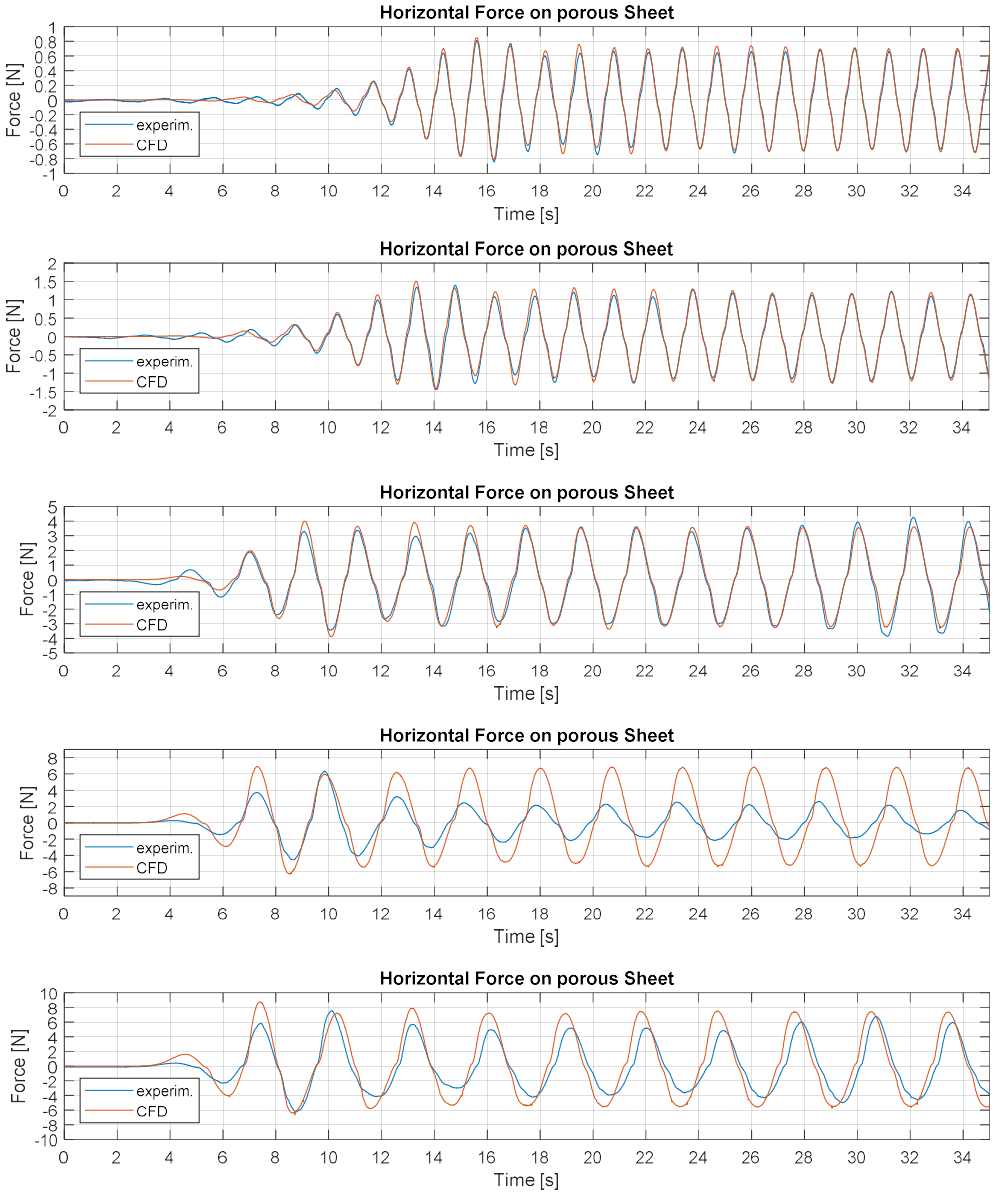

Fig. 8: Experimental and CFD results: time series of the horizontal force on the plate for the wave conditions F2, F3, F6, F9 and F10 (from top to bottom)

A_{Force} for the experimental and CFD results as well as the difference in percent. As before, the average force amplitude A_{Force} was analysed for the last 10 wave periods.

TABLE VI
AVG. AMPL. A_{FORCE} [N] FOR SELECTED WAVE CONDITIONS FOR THE MODELS WITH FLAT BOTTOM

	F2	F3	F6	F9	F10
Experimental	0.634	1.048	3.112	2.145	4.399
CFD	0.665	1.130	2.983	5.877	5.970
Diff. CFD/Exp. [%]	+4.9	+7.8	-4.2	+174.0	+35.7

The overall results show that the CFD model is able to reproduce the nonlinear pressure drop across the porous plate. For the wave conditions F2, F3 and F6 the CFD results match the experimental data very well, but the results for the wave condition F10 exhibit a larger discrepancy and for wave condition F9 the results are significantly different to the tank test results. For these frequencies, wave measurements at the plate location showed a significant increase from waves measured close to the inlet, indicating that there was a strong interaction between the wave and the ramp.

To study the influence of the bottom ramp with CFD, comparative simulations including the bottom ramp in the domain as shown in Fig. 1 were run for the wave conditions F2 and F9. The overall water depth was 1.17m, the depth above the ramp was 1.00m. The results are presented in Fig. 9 and Fig. 10, showing the time series of the horizontal force on the sheet, as well as Table VII, containing the average force amplitude A_{Force} for the models with and without the bottom ramp.

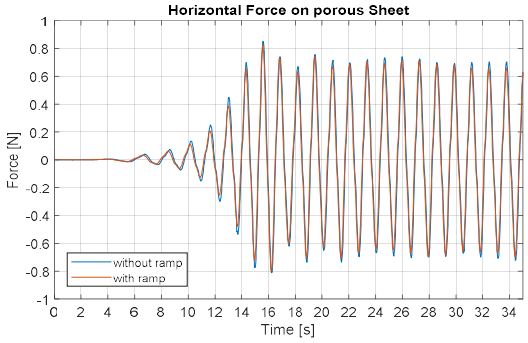

Fig. 9: Time series of the horizontal force on the plate for wave F2 with and without the bottom ramp

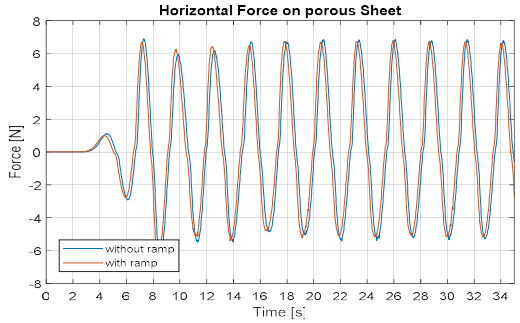

Fig. 10: Time series of the horizontal force on the plate for wave F9 with and without the bottom ramp

TABLE VII
EFFECT OF RAMP - AVG AMPL. A_{FORCE} [N]

	F2	F9
Flat Floor	0.665	5.877
With Ramp	0.635	5.739

The raised floor has the effect of decreasing the force amplitude by 4.5% for wave F2 and by 2.3% for wave F9. A decrease could be explained by a misalignment of the waves by the ramp, causing the vertical component of the force to increase and the horizontal one to decrease. However, the differences are considered to be small and within the uncertainty of the mesh convergence studies and would have been expected to be higher to match the trend of the tank test results. Future simulations will be conducted to investigate why the CFD model does not reproduce a stronger wave-ramp interaction and whether this effect occurs for other wave conditions.

VI. CONCLUSION

The development of a model set-up for wave interaction with thin porous structures has been introduced. Overall, the CFD models presented are able to produce results close to the tank test results and the nonlinear behaviour of the force on the plate. The result for the wave condition F9 is considered to be anomalous. However, comparisons between potential flow models and the tank test results showed a similar discrepancy at this frequency, whereas other frequencies showed good agreement [9]. This may be an effect of strong interactions between the ramp and the waves in the experiments. It has to be examined further whether the CFD model reproduces a stronger interaction for other wave frequencies. A comparative simulation with the application of a non-slip condition for the tank floor could be considered for instance.

Future work will also include the influence of the domain length and the comparison of CFD results against experimental results for various other wave conditions, both regular and irregular.

Although laminar flow conditions are considered to be valid, simulations with the application of various turbulence models will be conducted. This aims to quantify the expected effects. It is likely that the introduction of a turbulence model will cause some reduction in the wave height as the waves propagate along the tank. The introduction of turbulence may also influence the force on the porous sheet.

Regarding the general model improvement, an alternative wave absorption technique, such as the active absorption technique for intermediate and deep waters [25] as well as a combination of both the active method and passive relaxation method [26], will be considered.

After achieving a robust model set-up for two-dimensional thin sheets, the studies will be extended to three-dimensional domains for porous sheets and cylinders as well as floating objects.

ACKNOWLEDGEMENT

The tank tests were conducted at the wave flume at Dalian University of Technology (DUT) as part of the UK-China ORE project ResIn ("Resilient Integrated Coupled FOW Platform Design Methodology").

REFERENCES

[1] P. Higuera, "olaFlow: CFD for waves." 2017.

[2] P. Higuera, J. L. Lara, and I. J. Losada, "Three-dimensional interaction of waves and porous coastal structures using OpenFOAM®. Part II: Application," *Coast. Eng.*, vol. 83, pp. 259–270, 2014.

[3] E. B. L. Mackay, A. Feichtner, R. E. Smith, P. R. Thies, and L. Johanning, "Verification of a Boundary Element Model for Wave Forces on Structures with Porous Elements," 2017.

[4] Z. Huang, Y. Li, and Y. Liu, "Hydraulic performance and wave loadings of perforated/slotted coastal structures: A review," *Ocean Eng.*, vol. 38, no. 10, pp. 1031–1053, 2011.

[5] J. Dai, C. M. Wang, T. Utsunomiya, and W. Duan, "Review of recent research and developments on floating breakwaters," *Ocean Eng.*, vol. 158, no. April, pp. 132–151, 2018.

[6] M. J. Downie, J. Wang, and J. M. R. Graham, "The Effectiveness of Porous Damping Devices," *The Tenth International Offshore and Polar Engineering Conference*. International Society of Offshore and Polar Engineers, Seattle, Washington, USA, p. 8, 2000.

[7] C. P. Lee and W. K. Ker, "Coupling of linear waves and a hybrid porous TLP," *Ocean Eng.*, vol. 29, no. 9, pp. 1049–1066, 2002.

[8] B. Molin, "Hydrodynamic modeling of perforated structures," *Appl. Ocean Res.*, vol. 33, no. 1, pp. 1–11, 2011.

[9] E. Mackay, L. Johanning, D. Qiao, and D. Ning, "Numerical and Experimental Modelling of Wave Loads on thin porous Sheets," in *Proceedings of the ASME 2019 38th International Conference on Ocean, Offshore and Arctic Engineering*, 2019, pp. 1–10.

[10] P. Higuera, J. L. Lara, and I. J. Losada, "Three-dimensional interaction of waves and porous coastal structures using OpenFOAM. Part I: Formulation and validation," *Coast. Eng.*, vol. 83, pp. 243–258, 2014.

[11] C. W. Hirt and B. D. Nichols, "Volume of fluid (VOF) method for the dynamics of free boundaries," *J. Comput. Phys.*, vol. 39, no. 1, pp. 201–225, Jan. 1981.

[12] E. Berberovic, N. P. Van Hinsberg, S. Jakirlic, I. V Roisman, and C. Tropea, "Drop impact onto a liquid layer of finite thickness : Dynamics of the cavity evolution," *Phys. Rev. E*, vol. 79, no. 3, pp. 1–15, 2009.

[13] C. Greenshields, "OpenFOAM 2.3.0: Multiphase Modelling - Predictor-Corrector Semi-Implicit MULES," 2014. [Online]. Available: https://openfoam.org/release/2-3-0/multiphase/.

[14] J. Roenby, H. Bredmose, and H. Jasak, "A Computational Method for Sharp Interface Advection," *R. Soc. open sci.*, vol. 3, no. 160405, 2016.

[15] P. Higuera, J. L. Lara, and I. J. Losada, "Realistic wave generation and active wave absorption for Navier-Stokes models. Application to OpenFOAM®.," *Coast. Eng.*, vol. 71, pp. 102–118, 2013.

[16] C. K. Sollitt and R. H. Cross, "Laboratory investigations of rubble-mound breakwaters," *Coast. Eng. Proc.*, vol. 1, no. 13, 1972.

[17] F. Engelund, "On the laminar and turbulent flows of ground water through homogeneous sand." Akad. for de Tekniske Videnskaber, 1953.

[18] M. R. A. Van Gent, "Wave interaction with permeable coastal structures," *PhD Thesis, Delft Univ. Technol. Delft, Netherlands*, no. January 1995, 1995.

[19] B. Jensen, N. G. Jacobsen, and E. D. Christensen, "Investigations on the porous media equations and resistance coefficients for coastal structures," *Coast. Eng.*, vol. 84, pp. 56–72, 2014.

[20] L. F. Chen, J. Zang, A. J. Hillis, G. C. J. Morgan, and A. R. Plummer, "Numerical investigation of wave–structure interaction using OpenFOAM," *Ocean Eng.*, vol. 88, pp. 91–109, 2014.

[21] Z. Z. Hu, D. Greaves, and A. Raby, "Numerical wave tank study of extreme waves and wave-structure interaction using OpenFoam®," *Ocean Eng.*, vol. 126, no. August, pp. 329–342, 2016.

[22] L. Chen, L. Sun, J. Zang, and A. Hillis, "Numerical Simulation of Wave-induced Roll of a 2-D Rectangular Barge Using OpenFOAM," *29th Int. Work. Water Waves Float. Bodies*, pp. 1–4, 2014.

[23] E. J. Ransley, D. M. Greaves, A. Raby, D. Simmonds, M. M. Jakobsen, and M. Kramer, "RANS-VOF modelling of the Wavestar point absorber," *Renew. Energy*, vol. 109, pp. 49–65, 2017.

[24] E. R. Mansard, E.P.D.; Funke, "The Measurement of Incident and Reflected Spectra Using a Least Squares Method," pp. 154–172, 1980.

[25] P. Higuera, "Enhancing active wave absorption in RANS models," pp. 1–20, 2018.

[26] N. G. Jacobsen, D. R. Fuhrman, and J. Fredsoe, "A wave generation toolbox for the open-source CFD library: OpenFoam," *Int. J. Numer. Methods Fluids*, vol. 70, no. November 2011, pp. 1073–1088, 2011.